buildings

MDPI

Article

Experimental and Numerical Simulation Investigations on the Bearing Capacity of Stepped Variable-Section DX Piles under Vertical Loading

Jinsheng Cheng [1], Lei Tong [1], Chuanzhi Sun [2,*], Hanbo Zhu [2] and Jibing Deng [3]

[1] Suqian City Urban Construction Investment (Group) Co., Ltd., Suqian 223800, China; cheng_js@126.com (J.C.); tonglei8899@126.com (L.T.)
[2] School of Civil Engineering and Architecture, Suqian College, Suqian 223800, China; 19156@squ.edu.cn
[3] China Construction Fifth Engineering Bureau Co., Ltd., Changsha 410004, China; cscec5bhdgs@cscec.com
* Correspondence: schzh_xzh@163.com

Abstract: As a new type of pile, the bearing characteristics of stepped variable-section DX piles (multi-joint extruded and expanded piles) are quite complicated; thus, their design concepts and pile-forming processes are still in the exploration stage, and their application in actual engineering is not particularly mature. The settlement law and load transfer law of the variable section DX pile have not been studied deeply, and the values of the parameters of engineering design are not clear, which are the problems to be solved for the variable section DX pile. To solve the above problems, the present study on the bearing characteristics of stepped variable-section DX piles under vertical loading is of great scientific significance and engineering practical value. In this study, the bearing capacity of a DX pile with two variable steps was first analyzed experimentally. Then, the bearing capacity of variable cross-section DX piles and equal cross-section piles were simulated under the same soil conditions. Later, the numerical simulation results were compared with the experimental results to verify the validity and accuracy of the numerical models established in ABAQUS software. Finally, the bearing capacity of stepped variable-section DX piles in different soil layers was analyzed numerically to compare the effect of different soils on the compressive bearing capacity of piles. The results indicated that the load-bearing plates had a greater influence on the bearing capacity of the stepped variable-section DX piles. At the optimum variable section ratio, which was close to 0.9, DX piles had a good bearing capacity. The relative errors of the numerical simulation ultimate loads were below 10%, which verified the accuracy of the developed numerical model. The simulated ultimate load of the equal-section pile was the smallest. The vertical compressive bearing capacity and the effect of controlling settlement under the same level of load of the variable section DX pile in sandy soil were both better than those in silt soil. There was little difference between the bearing capacities of the piles with a load-bearing plate. The bearing capacity of the pile with two load-bearing plates was the best, which can be used in practical engineering.

Keywords: DX piles; stepped variable-section; load–settlement; soils; bearing capacity

Citation: Cheng, J.; Tong, L.; Sun, C.; Zhu, H.; Deng, J. Experimental and Numerical Simulation Investigations on the Bearing Capacity of Stepped Variable-Section DX Piles under Vertical Loading. *Buildings* **2024**, *14*, 3078. https://doi.org/10.3390/buildings14103078

Academic Editor: Duc-Kien Thai

Received: 2 August 2024
Revised: 11 September 2024
Accepted: 19 September 2024
Published: 26 September 2024

1. Introduction

In structural engineering, pile foundation as a traditional form of foundation has been used until now, and plays an increasingly important role. It is mainly used in the case of poor geological conditions or high building requirements, with small settlement and high bearing capacity [1–5]. Among them, grouted piles are widely used because of their advantages, such as the high bearing capacity of a single pile, easy control of construction depth, low cost, and low noise [6–10]. The reinforced concrete equal cross-section grouted piles, which are more frequently used in China [11–15], mainly rely on the end bearing force at the bottom of the pile and the friction force at the side of the pile to carry the load. The way to improve the bearing capacity of piles is to increase the pile end area and increase the

pile side friction resistance. The usual practice is to increase the pile diameter and increase the pile side area, but this practice is usually more difficult to construct and increases the project cost.

Figure 1a shows a stepped variable-section pile. Variable cross-section piles have an obvious squeezing effect on the soil layer during settlement, increasing the pile's lateral friction resistance [16,17]. When the pile is under pressure, the step form can play a certain bearing role in each soil layer, and then, combined with the pile end grouting process, it can improve the bearing performance of the pile. Variable cross-section form fully applies the axial force of the pile body gradually decreases from top to bottom under vertical load, and the distribution law of bending moment shear force under transverse load is also big at the top and small at the bottom, so as to save the material used for the pile body and reduce the cost of the project. Figure 1b shows a DX pile. DX piles can greatly increase the single-pile bearing capacity because the load-bearing plate improves the contact area between the pile body and the soil, which enhances the bearing performance, and the rotary excavation and squeezing and expanding equipment has the effect of squeezing and compacting the soil around the pile.

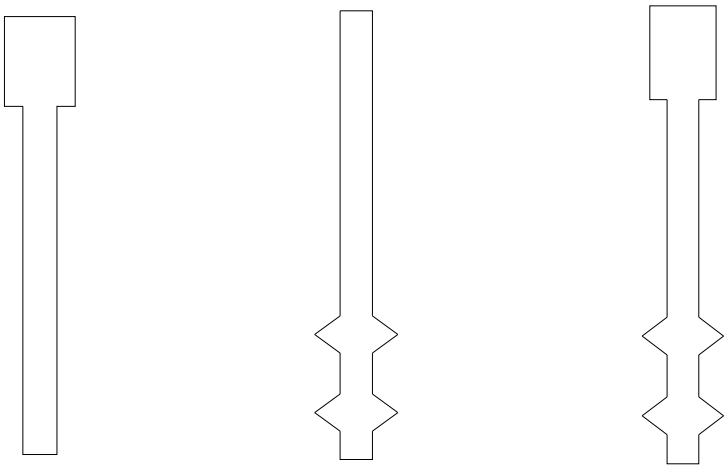

(**a**) A stepped variable-section pile (**b**) A DX pile (**c**) A stepped variable-section DX piles

Figure 1. Schematic diagram of piles.

On the basis of ensuring the safety and stability of pile foundations, it is a new challenge for the engineering community to meet the strict requirements of high quality, fast schedule and low cost on the project through theoretical and technological innovation. With this aim, many new forms of piling have been developed [18,19]. A stepped variable section DX pile [20] (named DX Pile after the inventor, Mr. Dexin He) is a new type of variable-section pile based on the combination of the advantages of both stepped variable section piles and DX piles, as shown in Figure 1c. It combines the advantages of both stepped variable-section piles and DX piles. It can fully mobilize the potential of pile–soil interaction and greatly improve the pile bearing capacity while reducing the cost. However, the design of stepped variable cross-section DX piles still adopts the recommended formula of the specification [21]. To meet the specification requirements, it is necessary to use the method of increasing the diameter of the pile body; this is not conducive to the construction progress and cost control. Therefore, how to ensure the stepped variable cross-section DX piles can ensure safety under vertical and horizontal loads as well as control the construction cost is a worthy research topic.

The stepped variable cross-section DX pile is subjected to pressure when it is affected by many factors, such as the pile type, material, and the influence of soil quality [22]. The bearing mechanism of the stepped variable cross-section DX pile is very complex under loading [23]. The study of pile–soil interaction on complex pile types is quite complicated. It

is very difficult to obtain accurate calculation results by the theoretical method of derivation of equations. The finite element numerical simulation calculation method has been widely used in the study of pile bearing mechanism, group pile effect, and pile–soil action. Finite element simulation can consider the aspects of nonlinearity, non-uniformity, and pile–soil contact properties of the soil so it can better reflect the actual situation. Ogura H. [24–26] studied a pile type similar to bamboo piles and carried out experiments in sandy soil to analyze the relationship between load and settlement. The results indicated that its bearing capacity was much higher than that of a straight-bore pile of the same diameter. Zhang et al. [27] proposed a numerical simulation method to consider the damaged area and parameters surrounding the pile based on field tests, indoor simulations, and damage theory. Based on the field test, Dong et al. [28] used ABAQUS finite element software to numerically simulate the experimental process of vertical load capacity test of a single pile of equal-section pile and variable-section pile. The results indicated that the average lateral friction resistance of variable section piles was larger than that of equal section piles, and the effect of lateral friction resistance of variable section piles is more advantageous than that of equal section piles.

As verified by several engineering examples, the step-type variable cross-section DX pile technology has the features of unique construction technology, advanced machinery, and simple construction process; reliable quality of bearing plate cavity and high bearing performance of single pile; and reduction of pile body materials to reduce the project cost [29]. However, the design of the step-type variable cross-section DX pile still adopts the recommended formula of the specification. To meet the specification requirements, the method of increasing the diameter of the pile body is adopted, which not only increases the difficulty of construction but also improves the project cost. Therefore, how to ensure the safety of stepped variable section DX piles under vertical or horizontal loads while controlling the construction cost is a topic worth studying. Therefore, based on the above purpose, the present study on the bearing characteristics of stepped variable-section DX piles under vertical compression has important scientific significance and practical value in engineering.

As a new type of pile, the bearing characteristics of stepped variable-section DX piles are quite complicated; thus, the design concept and pile-forming process are still in the exploration stage, and their application in actual engineering is not particularly mature. The settlement law and load transfer law of the variable section DX pile have not been studied deeply, and the values of the parameters of engineering design are not clear, which are the problems to be solved for the variable section DX pile. In this study, the bearing capacity of a DX pile with two variable steps was first analyzed experimentally. Then, combined with the experimental results in reference [30], numerical simulation analysis were carried out to analyze the bearing process of variable cross-section DX piles and equal cross-section piles under the same soil conditions by using ABAQUS finite element software. Later, the numerical simulation results were compared with the experimental results to verify the validity and accuracy of the numerical models. Finally, the bearing capacity of stepped variable-section DX piles in different soils was analyzed numerically to compare the effect of different soils on the compressive bearing capacity of piles. This study can promote the application and dissemination of stepped variable-section DX piles in practical engineering.

2. Design of Specimens and Experimental Program

2.1. Physical and Mechanical Properties of the Soil Samples

The soil used for the test was powdered soil from a site in Suqian as the model material for the foundation soil. After each layer of soil was compacted, soil samples (see Figure 2) were taken out around the model piles using the ring knife method to conduct geotechnical tests. Then, the physical and mechanical property indicators of the soil samples were obtained in Table 1.

Figure 2. Geotechnical test.

Table 1. Physical and mechanical properties of the soil samples.

Density	Specific Gravity of Soil Particles	Moisture Content	Cohesive Force	Angle of Internal Friction	Modulus of Compression	Poisson's Ratio
1.59 g/cm^3	2.72 g/cm^3	16.23%	15.12 kPa	25.4°	10.06 MPa	0.4

2.2. Design of Test Piles

The model design first observed the condition of geometrical similarity according to the actual engineering needs and then integrated the difficulty and cost of the test production, the actual conditions of the production equipment, the accuracy requirements of the test measurements, and other aspects of the considerations, which can ensure the accuracy of the test piles. Piles S1–S5 were from reference [30], and one pile, S6, was the experimental model in this study, which was made in the same batch as piles S1–S5. The diameter of the piles body was 50 mm, and the length of the piles was 1100 mm. The diameter of the load-bearing plate was 100 mm. The variable ratio b is the ratio of the lower pile diameter to the upper pile diameter. The location of the variable section was 500 mm from the top of the pile. The variable section pile adopted a stepped pile type. The number of load-bearing plates was 2 for pile S6, 1 for piles S2–S5, and 0 for pile S1. The position of the load-bearing plate of the pile S6 was 180 mm and 360 mm from the bottom of the pile. The parameters of the test piles are shown in Table 2. The material parameters of each pile body are shown in Table 3. Figure 3 shows the design drawing of piles S1–S6.

Table 2. Design parameters of test piles (Unit: mm).

No.	L	D_1	D_2	b	l_1	l_2	D_3
S1	1100	50	50	1	—	—	—
S2	1100	50	50	1	—	180	100
S3	1100	50	45	0.9	500	180	100
S4	1100	50	40	0.8	500	180	100
S5	1100	50	35	0.7	500	180	100
S6	1100	50	40	0.8	500	360/180	100

Note: L was the length of the pile; l_1 was the distance from the variable section to the pile top; l_2 was the distance from the load-bearing plate to the pile bottom; D_1 was the diameter of the pile top; D_2 was the diameter of the pile bottom; D_3 was the diameter of the load-bearing plate.

Table 3. Material parameters of pile body.

Pile Material	Density	Elastic Modulus	Poisson's Ratio
Pine wood	0.58 g/cm^3	5.4 GPa	0.3

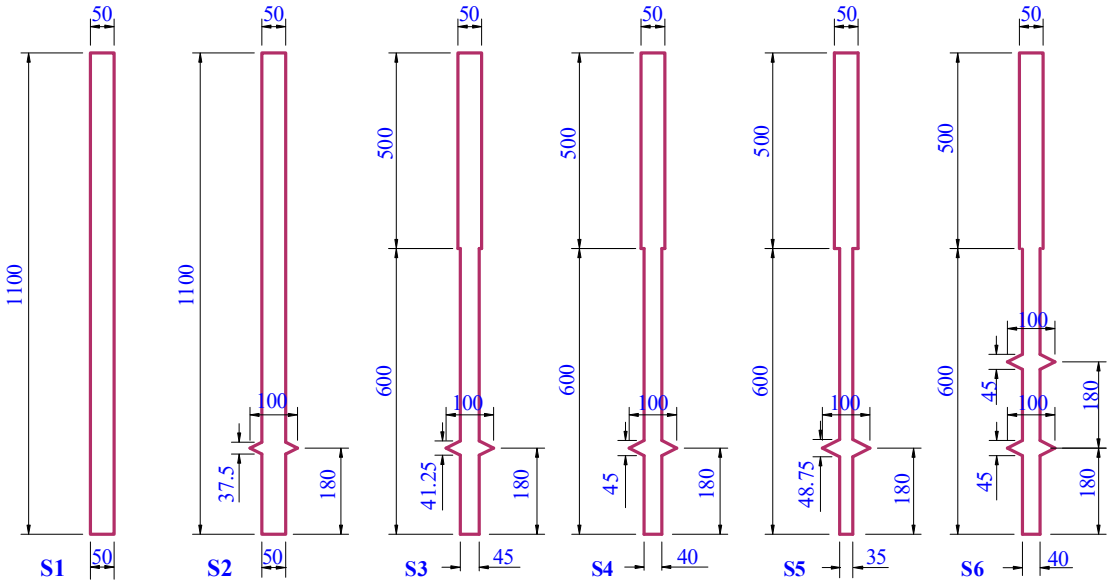

Figure 3. Design drawing of piles S1–S6.

2.3. Test Setup and Loading

The soil was first filled to a predetermined pile end height location. Then, the model pile was placed and secured at the designated location, and then the soil fill was continued to a predetermined pile top height. The model pile and soil pressure box were buried, as shown in Figure 4.

(**a**) A model pile (**b**) A soil pressure box

Figure 4. Buried photos.

To better simulate the actual environment for the test, the model box and the loading device were specially designed for this model test. The bottom edge of the model box measured 1.8 m × 1.8 m, and the height was 2 m. The bottom plate of the model box was cross-welded with channels, and the four directions of the middle plate of the model box each extended out to connect the channels of the loading device. The peripheral skeleton of the model box was made of equilateral angle steel welded together, and the wall of the box was made of steel plate with a thickness of 5 mm, which was designed as a flat type for filling and unloading the soil. The loading device was designed and produced by the lever principle. The column was connected to the chassis, and then the lever was connected to the column with an articulated connection. The other end of the lever hung an iron frame for placing the loading weights. To prevent the lever from tilting sideways during

the loading process so that the centralized force was eccentric, a limit on both sides of the lever was designed. The centralized force was applied by means of a removable screw mounted underneath with a spherical head. Under the condition of meeting the distance requirement, up to five model piles can be placed in two directions in the plane. When the test of one pile was finished, the mounting screw could be removed to carry out the loading test on another model pile. The model loading device diagram is shown in Figure 5. The vertical load model test loading mode adopted the slow sustaining load method in reference [5]. The vertical load was applied step by step incrementally during the test, and then the next level of load was added after each level of load reached relative stability until the model pile reached the ultimate load.

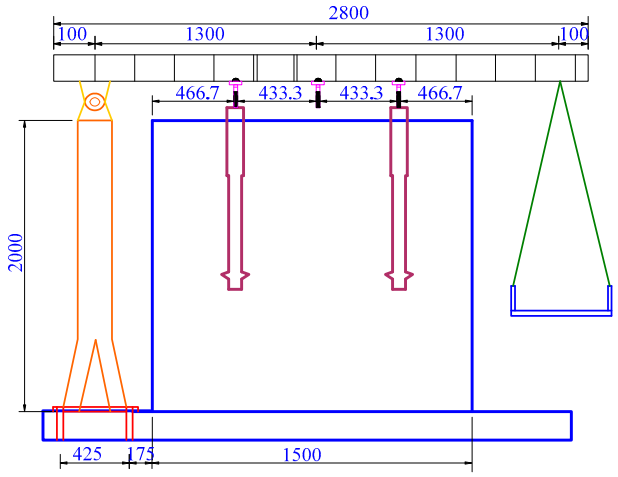

Figure 5. Loading device.

An electronic displacement meter with an accuracy of 0.01 mm was used to measure the settlement of the pile tops. Magnetic bearings held the displacement gauge to the channel steel, and the measurement point of the displacement gauge was set at the steel plate at the top of the pile. During the test loading, the corresponding displacement readings were recorded after each stage of load stabilization. Resistance strain gauges were pasted on each model pile to test the strain values. Ten pairs of strain gauges were arranged symmetrically on both sides of each pile body, totaling 20 gauges, and finally, the average value of the two sets of data was taken as the final value. The indicators of the strain gauges are shown in Table 4. The earth pressure measurement points were in the soil layer under the bearing plate, variable section, and pile end. When the soil was laid in layers, it was necessary to bury the earth pressure box at the measurement points, such as the bottom of the pile, the bottom of the bearing plate, and the variable section of each model pile, as shown in Figure 6. The main technical specifications of the earth pressure box used are shown in Table 5. A schematic diagram of the distribution of strain gauges in the pile, and the location of the earth pressure box is given in Figure 6.

Table 4. Indicators of strain gauges.

Model Number	Dimension	Resistance	Sensitivity Factor	Accuracy Class	Spring Tab
BK120-50AA	50 mm × 3 mm	119.5 ± 0.1 Ω	2.05 ± 1%	A	Half bridge

Table 5. Indicators of earth pressure boxes.

Scales	Bridge Pressure	Dimension	Sensitivity Factor
2 MPa	2 V	Φ20 mm × 10 mm	0.55

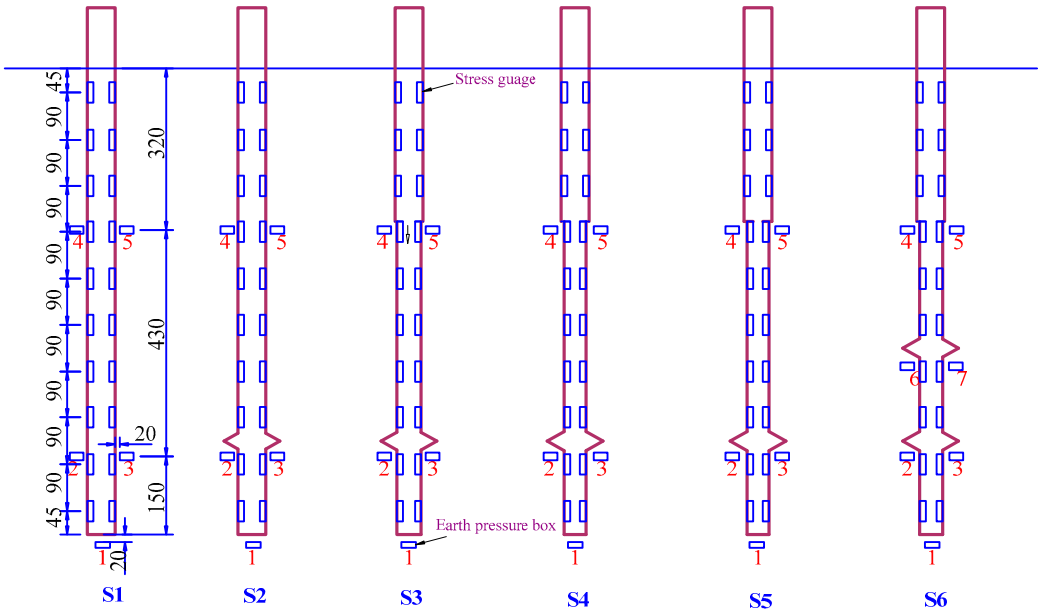

Figure 6. Distribution of strain gauges and locations of earth pressure boxes.

2.4. Experimental Results

2.4.1. Load–Settlement Curves

Load–settlement curves of piles S1–S6 are shown in Figure 7. Compared with the equal-section pile, the DX piles were obviously stronger in terms of settlement control. The presence of the load-bearing plate made the contact area between the pile and the soil body increase, and the lateral friction resistance of the pile body was greatly increased, thus increasing the bearing capacity of the pile. In the early stage of loading, when the load on the top of the pile was small, the settlement of stepped variable-section DX piles was similar to that of the equal section pile, and the advantages of stepped variable-section DX piles were gradually revealed with the increase of the load.

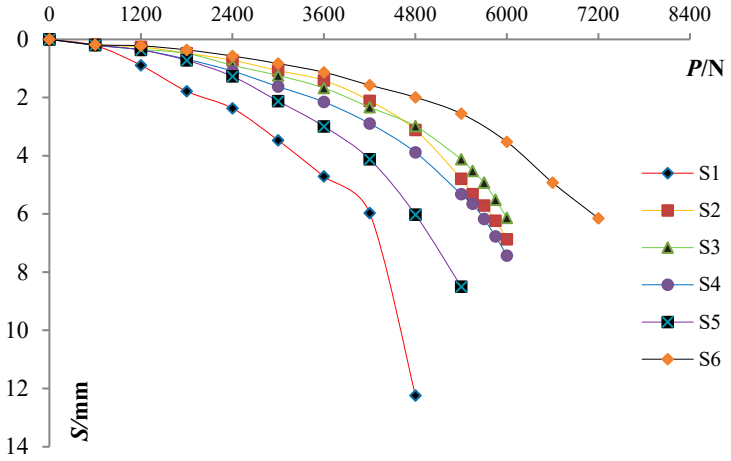

Figure 7. Load–settlement curves of piles.

2.4.2. Ultimate Load Capacity and Material Load Capacity per Unit Volume

To analyze and compare the efficiency of material use per unit volume of each pile, Q/V was introduced. In addition, the ratio of vertical bearing capacity Q_{si} of stepped variable-section DX piles to standard piles Q_{s1} and the ratio of volume V_{si} of stepped variable-section DX piles to standard piles V_{s1} (i is the number of each pile) were introduced to compare the changes in bearing capacity and material volume between DX piles, as shown in Table 6.

Table 6. Ultimate load capacity and material load capacity per unit volume.

Index	S1	S2	S3	S4	S5	S6
Q (N)	4200	5850	6000	5700	4800	7200
V (cm^3)	1766	1864	1655	1470	1307	1568
Q/V (N/cm^3)	2.4	3.1	3.6	3.9	3.7	4.5
Q_{si}/Q_{s1}	1.00	1.38	1.42	1.35	1.14	1.71
V_{si}/V_{s1}	1.00	1.06	0.94	0.83	0.74	0.88

From Table 6, the ultimate load of DX piles was higher than that of the equal section pile S1. The total volume of S2 piles with a DX load-bearing plate was increased by 6%, but its bearing capacity was increased by 38%. The bearing capacity of pile S3 was the most prominent among the DX piles with a DX load-bearing plate, and the ultimate load of the pile decreased gradually as the pile diameter ratio became smaller, among which the ultimate load of pile S5 decreased more obviously. It indicated that the factor of variable cross-section pile diameter ratio had a large influence on the bearing capacity of the DX pile. There was an optimal variable cross-section ratio, whose value was near 0.9, the DX piles exert a large bearing capacity. Pile S6 was a DX pile with two DX load-bearing plates. Its bearing capacity was higher than that of pile S3 with a DX load-bearing plate, indicating that the load-bearing plates played a greater role in improving the ultimate load of the pile.

The Q/V had an obvious correlation with the variable cross-section pile diameter ratio. As the variable cross-section ratio decreased, the ultimate capacity per unit volume first increased and then decreased. From the index of ultimate load per unit volume of material, the variable section pile diameter ratio cannot be too large to maximize the efficiency of material use. There was an optimal variable section ratio b, whose value was higher when b was near 0.8. The value of Q/V Pile S6 with two load-bearing plates was greater than the other DX piles with a load-bearing plate, and that of the equal-section straight pile S1 was the smallest, indicating that the load-bearing plates had a greater influence on the ultimate capacity per unit volume of the stepped variable-section DX piles.

2.4.3. Distribution Curves of Lateral Friction Resistance

Figure 8 shows the distribution of lateral friction resistance of pile S6. Compared with pile S4 in reference [30], variable section S6 pile had two load-bearing plates, and its lateral friction resistance was fully exerted. The sudden change of lateral friction resistance at the bearing discs can illustrate the great role of the bearing plate in the bearing of the pile body. With the gradual increase of loading, the relative displacement between the pile and the soil was also increased, the lateral friction resistance became larger, and the bearing plate was more fully utilized. When the pile settlement reached a certain level, there was a gap between the pile and the soil, and the soil was loosened, resulting in less lateral friction resistance at the top of the load-bearing plate.

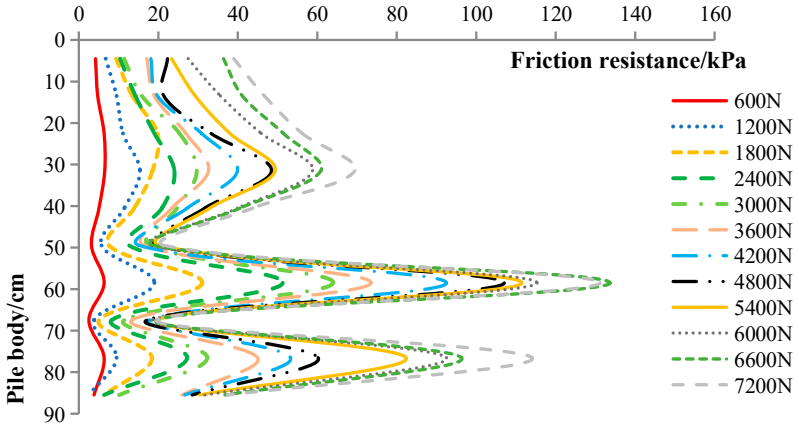

Figure 8. Distribution curves of lateral friction resistance of pile S6.

2.4.4. Earth Pressure

Figure 9 shows the variation curves of soil pressure at the pile end under vertical loading. Under the same vertical load, the soil pressure at the pile end of equal-section pile S1 was larger than that of DX piles S2–S6. The friction resistance of the pile body and load-bearing plate resistance of the DX pile bear a large portion of the pile body, which played a great role. The soil pressure at the pile end was very small, which can effectively control the settlement at the pile end. Among the various DX piles, the S6 pile had two load-bearing plates. Its soil pressure at the end of the pile was the smallest, and the advantage of settlement control was obvious. The soil pressures at the end of piles S2, S3, and S4 were small, indicating that a reasonable variable section was favorable to the bearing capacity of the piles. Pile S5, with a smaller *b* value, had larger soil pressure at the pile end and an obvious loss of bearing capacity.

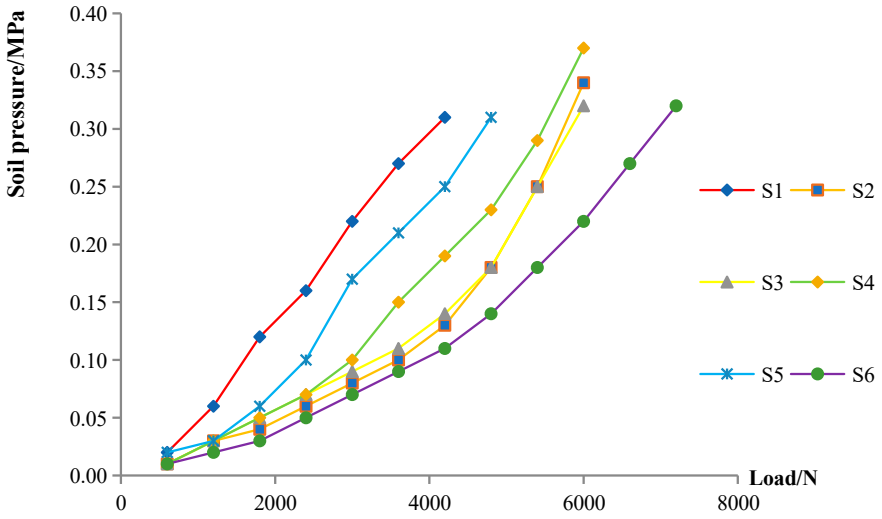

Figure 9. Soil pressure curves at the end of piles.

3. Finite Element Modeling of Pile Bodies

3.1. Basic Assumptions

(1) The pile body was rigid so that the pile body was not compressed by vertical pressure. The pile body was assumed to be modeled by linear elastic.
(2) The soil was assumed to be an isotropic elastic–plastic body, and the Mohr–Coulomb yield criterion was used.
(3) The friction coefficients between the units did not change during the modeling process.
(4) The effect of disturbance of the soil layer by factors such as the construction process was not considered.

3.2. The Constitutive Model of the Soil Body

The primary issue in the analysis of pile–soil problems was the selection of a constitutive model for the soil properties. The soil was assumed to be an isotropic elastic–plastic body, and the Mohr–Coulomb yield criterion was used.

The three widely used classical elastoplastic models are the Mohr–Coulomb model, the Druker–Prager model, and the Cambridge model. The Mohr–Coulomb model was used to simulate the pile–soil interaction. It can describe the material properties of geotechnical materials, such as the isotropic strain hardening and softening properties, and has been widely used in the simulation of geotechnical engineering. In the simple stress state, the Mohr–Coulomb yield criterion is

$$f(\sigma_1, \sigma_2, \sigma_3) = \frac{1}{2}(\sigma_1 - \sigma_3) + \frac{1}{2}(\sigma_1 + \sigma_3)\sin\psi - c\cos\psi = 0 \quad (1)$$

where σ_1, σ_2, σ_3 refer to the first principal stress, the second principal stress, and the third principal stress; c and Ψ must refer to the cohesion and the angle of internal friction, respectively.

As shown in Figure 10, the friction angle φ also indicates the shape of the yield surface of the material on the π-plane, and when $\varphi = 0°$, the Mohr–Coulomb model is transformed into the Tresca model, which is independent of the peripheral pressure, and at this time, the yield surface on the π-plane exhibits an ortho-hexagonal shape. At $\varphi = 90°$, the Mohr–Coulomb model is transformed into the Rankine model when the yield surface of the π-plane presents a positive triangle and $R_{mc} \to \infty$. If $0° \leq \varphi \leq 90°$, then the yield surface presents a hexagonal shape with equal sides but not equal angles, which is called the Mohr–Coulomb hexagon.

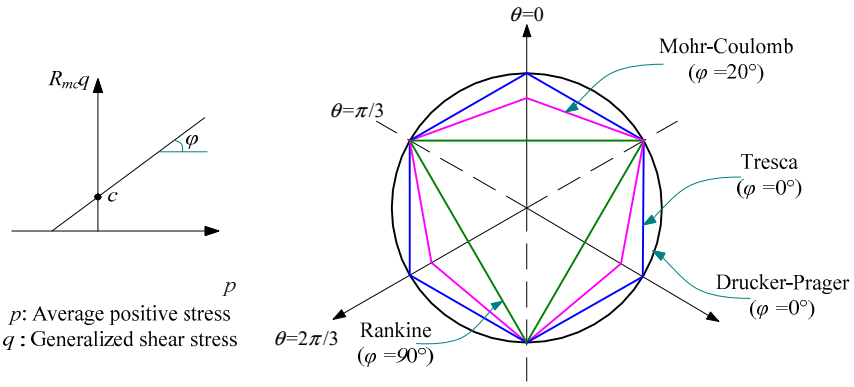

Figure 10. Meridian plane and deviatoric stress plane yield surface shape.

3.3. The Constitutive Mode of the Pile Body

The pile body was rigid so that the pile body was not compressed by vertical pressure. The pile body was assumed to be modeled by linear elastic. The constitutive relation is

$$\sigma_{ij} = \left[\frac{2G\mu}{1-2\mu}\delta_{ij}\delta_{kl} + G\left(\delta_{ik}\delta_{jl} + \delta_{il}\delta_{jk}\right)\right]\varepsilon_{kl} = D_{ijkl}\varepsilon_{kl} \tag{2}$$

where E is the elastic modulus of the material, μ is the Poisson's ratio of the material, $G = E/2(1+\mu)$, D_{ijkl} is the component of the elasticity tensor, and the matrix form of D_{ijkl} is

$$D = \frac{E}{(1+\mu)(1-2\mu)}\begin{bmatrix} 1-\mu & \mu & \mu & 0 & 0 & 0 \\ & 1-\mu & \mu & 0 & 0 & 0 \\ & & 1-\mu & 0 & 0 & 0 \\ & & & \frac{1}{2}-\mu & 0 & 0 \\ & & & & \frac{1}{2}-\mu & 0 \\ & & & & & 0 \end{bmatrix} \tag{3}$$

3.4. Finite Element Modeling

According to the actual dimensions of the pile and the soil body of the model test, the soil body around the pile was a rectangular body of 1.8 m × 1.8 m × 2 m, the outer diameter of the pile body was 0.05 m, the length of the pile was 1.1 m, and the depth of the pile below the soil layer was 0.9 m. The model with 1/4 symmetry was established. The pile body was modeled as shown in Figure 11a. The model space was selected as three-dimensional (3D), and its type was deformable. The shape in the basic features was selected as solid and its type was rotated. The model space of the soil body was also selected as 3D, and its type was deformable. The shape in the basic features was selected as solid and its type was stretched. The soil body of the rectangular body was modeled, and then the geometric elements were split to divide the soil part where the pile was located, and the soil body was established, as shown in Figure 11b. A linear elastic model was used for the pile, and

an isotropic elastoplastic body was selected for the soil. The material modeling parameters of the pile and soil are shown in Tables 1 and 3.

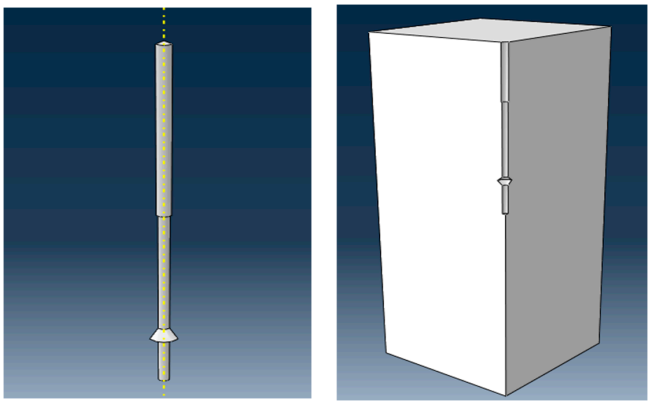

(**a**) Pile model (**b**) Soil model

Figure 11. Establishment of the pile–soil model.

After defining the material properties of the parts, they were assembled in the assembly module, where the parts were assembled into a whole by means of different positioning relationships. The contact module was utilized to define the contact units. Face-to-face contact was selected to create contact surfaces for each component, and then a master–slave algorithm was used to create contact pairs. A softer soil material was selected for the follower surface. The soil surface and the pile surface were set up as bound lifts that would not be displaced relative to each other. ABAQUS software has three main meshing techniques: free meshing, structured meshing, and swept meshing. Both the pile model and the soil model were meshed by the swept mesh technique using linear C3D8R units. The meshing was completed, as shown in Figure 12. Applying loads and boundary constraints was performed in the loading module. The boundary conditions for the numerical model were vertical displacement and bottom radial selection constraints for the soil model, and radial displacement selection constraints for the side parts of the soil model. To study the stress–strain relationship of the model, the magnitude curve should be added after selecting the load type. The type of the curve was a tabular magnitude curve, which determined the increase of the load at each time point, and the size and sequence of loading were based on the experimental pile.

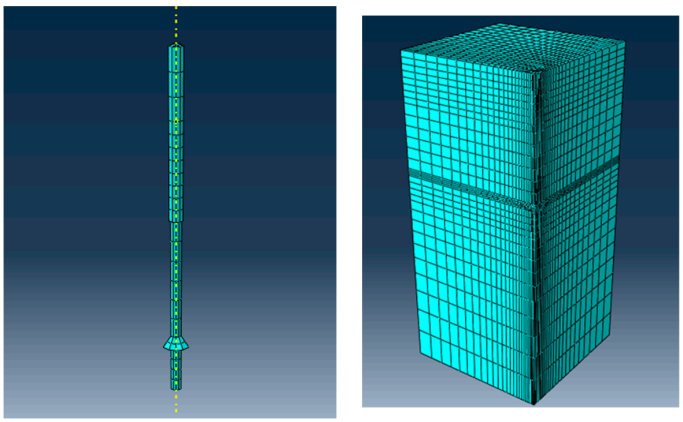

(**a**) Pile model (**b**) Soil model

Figure 12. Schematic diagram of meshing.

3.5. Validation of Numerical Results

Numerical simulation analysis was conducted on the equal-section pile S1, the DX pile S2, and stepped variable-section DX piles S4 and S6. Figure 13 shows the comparison of

experimental and numerical simulation load–settlement curves. The experimental values and simulation values of the ultimate load existed within a certain allowable error; this was because the numerical simulation of the parameter value was generally idealized, while in the actual experiment, there were many uncontrollable factors, such as uneven soil layer densities, etc., which caused errors, but the experimental and numerical simulation load–settlement curves overlapped. The experimental and numerical simulation ultimate loads were compared in Table 7. From Table 7, it can be seen clearly that the relative errors of the numerical simulation results were below 10%, which validated the accuracy of the finite element model.

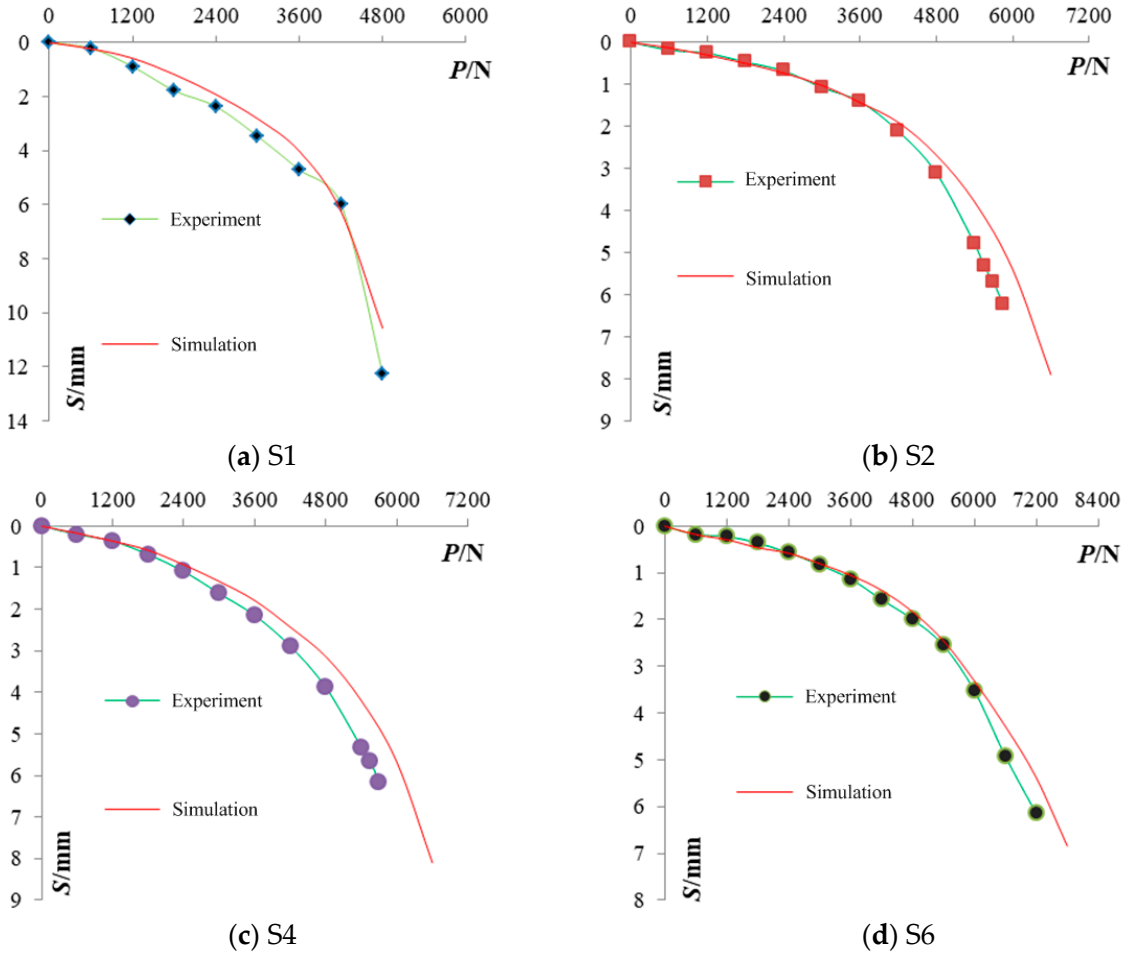

Figure 13. Comparison of experimental and numerical simulation load–settlement curves.

Table 7. Comparison of experimental and numerical simulation ultimate loads.

No.	Experiment E_e/N	Simulation S/N	Relative Error $E_r = (S - E_e)/E_e$
S1	4200	4100	–2.4%
S2	5850	6300	7.7%
S4	5700	6200	8.8%
S6	7200	7500	4.2%

3.6. Finite Element Results

3.6.1. Stress Analysis of the Pile Body

When the vertical load at the pile top was 4.2 kN, the stress cloud of each pile body was simulated, as shown in Figure 14. Under vertical pressure, the stress of the equal-section pile S1 gradually decreased from top to bottom, the stress of DX pile S2 also decreased from top to bottom, and the decrease at the bearing plate was obviously accelerated, indicating

that a large portion of the load was transmitted to the soil around the pile through the bearing plate. Variable-section piles S4 and S6 had reduced cross-sectional area at the variable section and higher stresses, and the stress decreasing above and below their load-bearing plates was obvious. Compared with the equal-section pile S1, the axial force in the area below the bearing plate of the variable cross-section DX pile was extremely small, indicating that most of the load had been transferred to the soil around the piles, and the soil pressure at the bottom of the piles was small, which can effectively control the settlement of the piles, and reflected the advantages of variable cross-section DX piles in bearing.

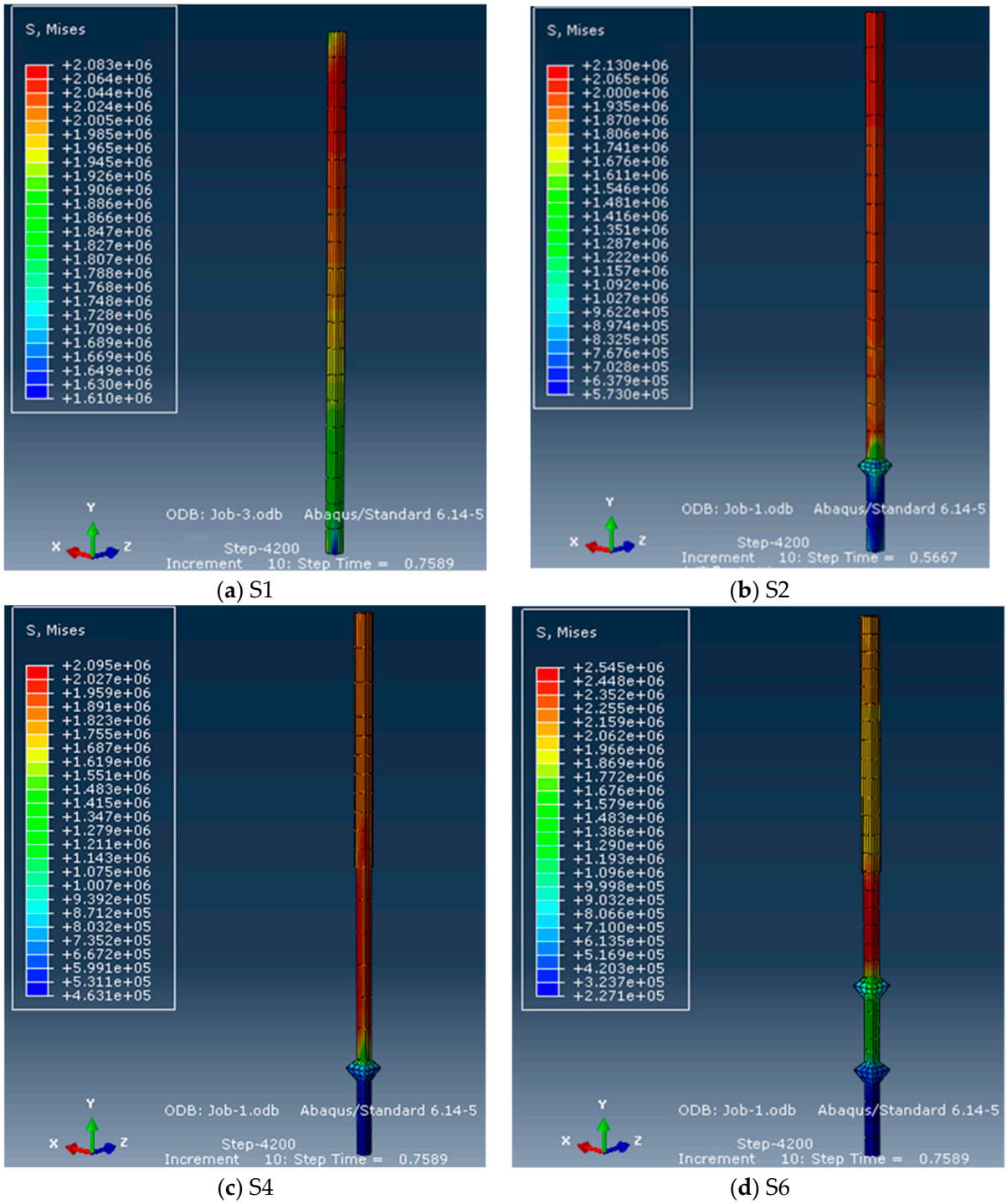

(**a**) S1 (**b**) S2

(**c**) S4 (**d**) S6

Figure 14. Stress cloud maps of piles.

3.6.2. Soil Pressure around Piles

When the vertical load at the pile top was 4.2 kN, the stress cloud of soil around piles was simulated, as shown in Figure 15. The soil around the pile took more load transfer and played a great role in bearing. The soil stress at the load-bearing plate and variable section of the variable section DX pile was larger, while the soil stress on the pile side of the equal section pile was very small, indicating that in the process of pile bearing, due to the existence of the variable section and the load-bearing plate, it made a large part of the load to be transferred to the soil around the pile through the end-bearing action, which reduced the axial force of the pile end, and thus played a great role in the pile bearing. The soil pressure at the pile end of the equal-section straight piles was the largest, indicating that the equal-section straight pile was easy to settle and subside, while the soil pressure at the pile end of the DX piles was significantly increased, indicating that the stepped variable-section DX piles were advantageous for the control of pile settlement, and with the increase in the number of load-bearing plates, the bearing capacity of the stepped variable-section DX pile became better.

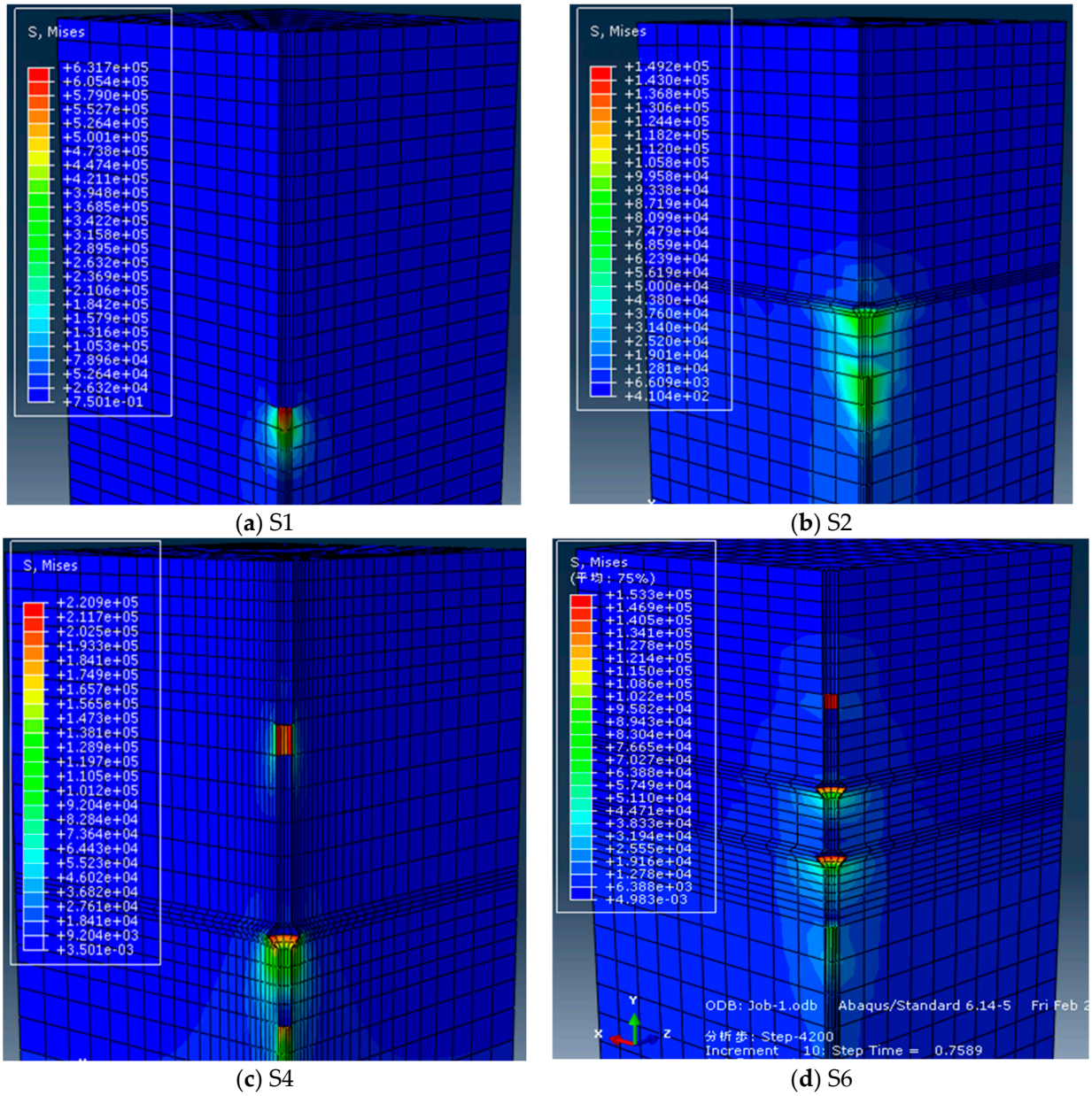

Figure 15. Stress cloud maps of soil around piles.

3.6.3. Compressive Bearing Capacity of a Pile in Different Soil Layers

Various parameters of the soil were varied to simulate and analyze the pile-bearing process in different soil layers. The parameters of silt soil and sandy soil are shown in Table 8. The load–settlement curves of piles in pulverized soil and sandy soil are shown in Figure 16. The settlement of pile S4 was the largest in the preloading period, and that of pile S2 was accelerated in the later period. There was not much difference between the two ultimate loads. The bearing capacity of stepped variable-section DX piles in sandy soil was stronger than that in silt soil. The settlements of the three-stepped variable-section DX piles in sandy soil were smaller than those in silt soil, indicating that the piles were more effective in resisting compressive bearing in sandy soil than in pulverized soil.

Table 8. Parametric soil test parameters for silt and sandy soils.

Name	Density /(g/cm^3)	Specific Gravity of Particles /(g/cm^3)	Water Content	*c* /kPa	Ψ /°	*E* /MPa	*μ*
Silt soil	1.59	2.72	16.23%	15.12	25.4	10.06	0.4
Sandy soil	1.79	2.65	1.65%	4.27	16.2°	34.3	0.4

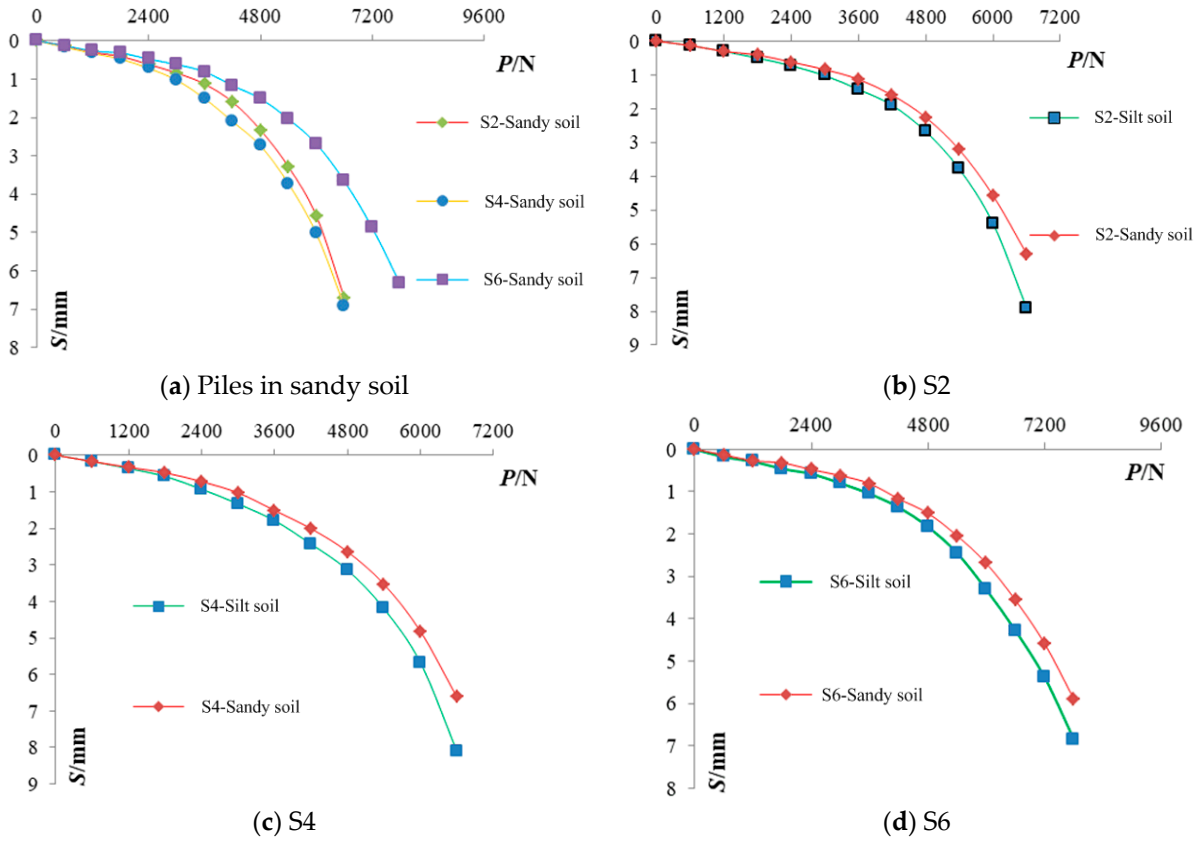

(**a**) Piles in sandy soil (**b**) S2

(**c**) S4 (**d**) S6

Figure 16. Load–settlement curves of the piles in different soil layers.

4. Conclusions

The bearing capacity of a DX pile with two variable steps was first analyzed experimentally. Then, the bearing capacity of variable cross-section DX piles and equal cross-section piles were simulated under the same soil conditions. Later, the numerical simulation results were compared with the experimental results to verify the validity and accuracy of the numerical models. Finally, the bearing capacity of stepped variable-section DX piles in different soils was analyzed numerically to compare the effect of different soils on the compressive bearing capacity of piles. This study can promote the application and dissemination of stepped variable-section DX piles in practical engineering.

The main conclusions were as follows.

1. Piles S1–S5 were from reference [30], and one pile, S6, was the experimental model in this study, which was made in the same batch with piles S1–S5. The diameter of the piles body was 50 mm, and the length of the piles was 1100 mm. The diameter of the load-bearing plate was 100 mm. The variable ratio b was the ratio of the lower pile diameter to the upper pile diameter, which took the values of 0.7, 0.8, 0.9, and 1. The location of the variable section was 500 mm from the top of the pile. The variable section pile adopted a stepped pile type. The number of load-bearing plates was 2 for pile S6, 1 for piles S2–S5, and 0 for pile S1;
2. The load-bearing plates had a greater influence on the bearing capacity of the stepped variable-section DX piles. At the optimum variable section ratio, which is close to 0.9, DX piles had a high bearing capacity. The bearing capacity of stepped variable-section DX piles with two variable steps was improved and its bearing capacity was best. The sudden change of lateral friction resistance at the bearing discs can illustrate the great role of the bearing plate in the bearing of the pile body. The soil pressure at the end of the pile with two variable steps was the smallest, and its settlement control was obvious;
3. The experimental values and simulation values of the ultimate load existed within a certain allowable error; this was because the numerical simulation of the parameter value was generally idealized, while in the actual experiment, there were many uncontrollable factors such as uneven soil layer densities, etc., which caused errors, but the experimental and numerical simulation load–settlement curves overlapped. The relative errors of the numerical simulation ultimate loads were below 10%, which verified the accuracy of the developed numerical model;
4. The simulated ultimate load of the equal-section pile was the smallest. The effect of settlement control of equal-section piles was poor. Due to the existence of the load-bearing plate, the ultimate load of the piles with a bearing plate was greatly improved. The piles with two load-bearing plates had the highest bearing capacity;
5. The vertical compressive bearing capacity and the effect of controlling settlement under the same level of load of the variable section DX pile in sandy soil were both better than those in silt soil. There was little difference between the bearing capacities of the piles with a load-bearing plate. The bearing capacity of the pile with two load-bearing plates was the best.

Author Contributions: Conceptualization, C.S.; methodology, J.D; software, J.C.; validation, J.D.; formal analysis, L.T.; investigation, L.T.; resources, J.C.; data curation, L.T.; writing—original draft preparation, J.C.; writing—review and editing, C.S.; visualization, H.Z.; supervision, C.S.; project administration, C.S.; funding acquisition, C.S. All authors have read and agreed to the published version of the manuscript.

Funding: This research has been supported by the Natural Science Research Project of Jiangsu Province Colleges and Universities (21KJD560002 and 23KJA560007), China; Research and Innovation Team Project of Suqian College (2021TD04), China; Suqian Sci & Tech Program (H202313), China; Jiangsu Civil Architecture Society project ((2023) No. 4 Item 9), China; the Youth Fund Project of Suqian College (2023XQNA03), China; and the Fifth Provincial Research Funding Project of "333 High-level Talent Training" in 2020 (BRA2020241), China.

Data Availability Statement: The data presented in this study are available in the article here.

Conflicts of Interest: Author Jinsheng Cheng and Lei Tong were employed by the company Suqian City Ur-ban Construction Investment (Group) Co. Author Jibing Deng was employed by the company China Construction Fifth Engineering Bureau Co. The remaining authors declare that the research was conducted in the absence of any commercial or financial relationships that could be construed as a potential conflict of interest.

References

1. Zhao, X.Q.; Gong, X.N.; Duan, Y.; Guo, P. Load-bearing performance of caisson-bored pile composite anchorage foundation for long-span suspension bridge: 1-g model tests. *Acta Geotech.* **2023**, *18*, 3743–3763. [CrossRef]
2. Hassan, I.; Mohamedelhassan, E. Enhancing the load-bearing capacity of H-pile foundation by using electrokinetic treatment. *Int. J. Civ. Eng.* **2023**, *21*, 991–1005. [CrossRef]
3. Kumar, M.; Kumar, D.R.; Khatti, J.; Samui, P.; Grover, K.S. Prediction of bearing capacity of pile foundation using deep learning approaches. *Front. Struct. Civ. Eng.* **2024**, *18*, 870–886. [CrossRef]
4. Gao, F.; Wang, W.; Lv, Q.; Cheng, X. Experimental study on the bearing characteristics of rigid-flexible long-short pile composite foundations in thick collapsible loess areas. *KSCE J. Civ. Eng.* **2024**, *28*, 1690–1701. [CrossRef]
5. Kumar, A.; Kumar, S. Settlement based load-bearing in a combined pile–raft foundation. *Geotech. Geol. Eng.* **2024**, *42*, 1405–1421. [CrossRef]
6. Igoe, D.; Spagnoli, G.; Doherty, P.; Weixler, L. Design of a novel drilled-and-grouted pile in sand for offshore oil & gas structures. *Mar. Struct.* **2014**, *39*, 39–49.
7. Zhou, J.; Gong, X.; Naggar MH, E.; Zhang, R. Field study on the behavior of pre-bored grouted planted pile with enlarged grout base. *Acta Geotech.* **2021**, *16*, 3327–3338. [CrossRef]
8. Wan, Z.; Dai, G.; Gong, W. Study on the response of postside-grouted piles subjected to lateral loading in calcareous sand. *Acta Geotech.* **2022**, *17*, 3099–3115. [CrossRef]
9. Cao, S.; Wang, Q.; Ma, J.; Xiao, Z.; Li, C.; Yang, Y.; Wang, J. Experimental Investigation of Vertical Bearing Characteristics of Composite Post-grouting Piles in Sandy Soil. *Int. J. Civ. Eng.* **2024**, *22*, 303–315. [CrossRef]
10. Salem, T.N.; El-Basset, O.H.A.; Hassan, R. 3D Numerical Analysis of Post-Grouted Piles. *Indian Geotech. J.* **2024**, *54*, 1562–1583. [CrossRef]
11. Wan, Z.; Dai, G.; Gong, W. Field study on post-grouting effects of cast-in-place bored piles in extra-thick fine sand layers. *Acta Geotech* **2019**, *14*, 1357–1377. [CrossRef]
12. Wen, L.; Kong, G.; Li, Q.; Zhang, Z. Field tests on axial behavior of grouted steel pipe micropiles in marine soft clay. *Int. J. Geomech.* **2020**, *20*, 06020006. [CrossRef]
13. Huang, Y.; Zhuang, X.; Wang, P.; Zong, Z.L. Axial behavior of pressure grouted helical piles installed in marine soft clay based on full-scale field tests. *Geotech. Geol. Eng.* **2022**, *40*, 5799–5812. [CrossRef]
14. Zhou, Z.; Xu, F.; Lei, J.; Bai, Y.; Chen, C.; Xu, T.; Zhang, Z.; Zhu, L.; Liu, T. Experimental study of the influence of different hole-forming methods on the bearing characteristics of post-grouting pile in Loess Areas. *Transp. Geotech.* **2021**, *27*, 100423. [CrossRef]
15. Zhang, Y.; Bi, J.; Bai, X.; Yan, N.; Sang, S.; Lin, Z.; Wang, B.; Chen, J.; He, L. Test on bearing capacity of mudstone foundation and rock-socketed pile. *Sci. Technol. Eng.* **2023**, *23*, 722–730.
16. Zhuang, Y.; Song, K.; Easa, S.; Song, Y. Soil Interaction of H-shaped steel-RC stepped pile of integral abutment bridge: Experimental evaluation. *KSCE J. Civ. Eng.* **2023**, *27*, 1174–1190. [CrossRef]
17. Chen, L.; Zhuang, Y.; Song, K.; Easa, S.M.; Zhu, H. Novel HS-RC stepped pile foundation: Experimental and numerical evaluation. *Ocean Eng.* **2024**, *299*, 117196. [CrossRef]
18. Zyka, K.; Mohajerani, A. Composite piles: A review. *Constr. Build. Mater.* **2016**, *107*, 394–410. [CrossRef]
19. Wu, J.; Sun, F.; El, N.M.H.; Zhao, S.; Wang, K. Analytical solution for consolidation of sand-filled nodular pile (SFNP) foundation and its engineering application. *Int. J. Numer. Anal. Methods Geomech.* **2022**, *46*, 3236–3255. [CrossRef]
20. Wang, M.; He, D.; Tang, S. New pile foundation technology of 21 century: DX pile. *Eng. Sci.* **2021**, *14*, 4–12.
21. *JGJ 94-2008*; Industry Standard of the People's Republic of China. Technical Code for Building Pile Foundation. China Construction Industry Press: Beijing, China, 2008.
22. Qian, C.; Chen, L.; Tans, S.; Chai, X. Model test method of DX pile. *J. Beijing Jiaotong Univ.* **2012**, *36*, 85–89.
23. Wu, P.; Zhang, D.; Liu, Y.; Li, H.; Wang, Y. Model test on bearing characteristics of DX rock-socketed pile with bearing plate in strata. *J. Beijing Jiaotong Univ.* **2012**, *47*, 26–34.
24. Ogura, H. Study on bearing capacity of nodular cylinder pile by scaled model test. *J. Struct. Eng.* **1987**, *374*, 87–97.
25. Ogura, H. Study on bearing capacity of nodular cylinder pile by full-scale test of jacked piles. *J. Struct. Eng.* **1988**, *386*, 66–77.
26. Ogura, H. A theoretical analysis on load-settlement behavior of nodular piles. *J. Struct. Eng.* **1988**, *303*, 152–164.
27. Zhang, Y.; Wang, F.; Bai, X.; Yan, N.; Sang, S.; Kong, L.; Zhang, M.; Wei, Y. Numerical Simulation of Bearing capacity of Bored Piles in Mudstone Based on Zoning Assignment of Soil around Piles. *Buildings* **2022**, *12*, 1877. [CrossRef]
28. Dong, Q.; Xiao, Z.; Tang, D. Experimental Analysis of Vertical Bearing capacity of Piles with Different Variable Sections. *J. Wuhan Inst. Technol.* **2021**, *43*, 436–441.

29. Guo, P. Experimental Study on Bearing Characteristic and Failure Mechanism of Rock-Socketed DX Pile. Master's Thesis, Beijing Jiaotong University, Beijing, China, 2017.
30. Wang, Z.; Liu, J.C.; Gu, C.; Sun, C.Z. Model Test Study on vertical static bearing behaviors of DX pile with stepped variable cross-section. *Sci. Technol. Eng.* **2018**, *18*, 67–72.